Journal of Alloys and Compounds, 190 (1993) 171–179
JALCOM 402

Nuclear magnetic resonance study of the electronic structure and hydrogen motion in the random b.c.c.-TaV_2–H(D) system

A. V. Skripov, M. Yu. Belyaev and A. P. Stepanov
Institute of Metal Physics, Urals Branch of the Academy of Sciences, Ekaterinburg 620219 (Russian Federation)

L. N. Padurets and E. I. Sokolova
Institute of General and Inorganic Chemistry, Russian Academy of Sciences, Moscow 117907 (Russian Federation)

(Received April 1, 1992; in final form June 29, 1992)

Abstract

Nuclear magnetic resonance measurements of the ^1H, ^2D and ^{51}V spin–lattice relaxation times and Knight shifts in the random b.c.c.-$TaV_2H_x(D_x)$ system ($0.1 \leqslant x \leqslant 2.4$) have been performed over the temperature range 11–440 K. The relaxation data are analysed to obtain the parameters of H(D) diffusion, which is governed by a distribution of activation energies. The long-range diffusion of H(D) in b.c.c.-$TaV_2H_x(D_x)$ is found to be much faster than in C15-type $TaV_2H_x(D_x)$ with comparable H(D) contents. For all the studied samples (including those with mixed isotope composition) there is a distinct isotope effect on the average activation energy: $E_a^D > E_a^H$. The measured values of the Knight shifts and the electronic (Korringa) contributions to the spin–lattice relaxation rates indicate that the density of d-electron states at the Fermi level decreases with increasing H(D) content.

1. Introduction

TaV_2 may be prepared as a random b.c.c. alloy or as an intermetallic compound with the C15-type structure. Both crystalline modifications absorb considerable amounts of hydrogen [1]. Thus the TaV_2–H(D) system provides the opportunity to study the effects of the host metal structure on the hydrogen mobility and hydrogen-induced changes in the electronic properties. In previous papers we have reported the results of nuclear magnetic resonance (NMR) studies of H(D) motion [2, 3] and the electronic structure [4] of C15-type $TaV_2H_x(D_x)$. The aim of the present work is to investigate the hydrogen mobility and electronic properties of the random b.c.c.-$TaV_2H_x(D_x)$ system and to compare them with those of the C15-type modification. Since nuclear spin relaxation measurements have revealed the anomalous low temperature localized motion of H(D) atoms in C15-$TaV_2H_x(D_x)$ [2, 3], it is of special interest to check if such motion exists in the random b.c.c. system of the same composition.

The important feature of b.c.c. alloy–hydrogen systems is the suppression of hydride phase precipitation. In fact, for these ternary systems the region of the homogeneous solid solution (α) phase is much broader than for binary b.c.c. metal–hydrogen systems [5, 6]. This is favourable for studies of hydrogen mobility as a function of temperature and hydrogen content.

In order to elucidate the mechanisms of hydrogen diffusion, it is important to investigate isotope effects in hydrogen motion [7, 8]. The particularly interesting question is whether the hydrogen diffusion parameters are changed when the isotope substitution is only partial. The corresponding experimental data may clarify the role of the interaction between diffusing atoms at high hydrogen concentrations. We have measured the ^1H, ^2D and ^{51}V spin–lattice relaxation times T_1 in b.c.c.-$TaV_2H_x(D_x)$ (including samples with mixed isotope composition) over wide ranges of temperature, hydrogen content and resonance frequency. The experimental data are analysed to obtain the H(D) diffusion parameters. We also discuss the H(D) concentration dependence of the density of electron states at the Fermi level, as derived from measurements of the ^1H and ^{51}V Knight shifts and the electronic (Korringa) contribution to the ^{51}V spin–lattice relaxation rate.

2. Experimental details

The random b.c.c.-TaV_2 alloy was prepared by arc melting appropriate amounts of the high purity metals in a helium atmosphere. The samples were charged with $H_2(D_2)$ gas at a pressure of about 1 bar using a Sieverts-type vacuum system. The H(D) content was determined from the hydrogen pressure change in the

0925-8388/93/$6.00

TABLE 1. Compositions and lattice parameters of the studied b.c.c.-$TaV_2H_x(D_x)$ samples at room temperature

Sample	a (Å)
b.c.c.-$TaV_2H_{0.1}$	3.135
b.c.c.-$TaV_2H_{0.2}D_{0.4}$	3.156
b.c.c.-$TaV_2D_{1.2}$	3.176
b.c.c.-$TaV_2H_{0.5}D_{1.0}$	3.200
b.c.c.-$TaV_2H_{1.8}$	3.219
b.c.c.-$TaV_2H_{2.3}$	3.239
b.c.c.-$TaV_2D_{2.4}$	3.241

calibrated volume of the system. In order to prepare mixed isotope samples, we used an H_2–D_2 gas mixture, the H:D ratio in the sample being estimated from the intensities of the ^1H and ^2D NMR signals. X-ray diffraction studies have shown that at room temperature all the samples are single-phase solid solutions with a b.c.c. host metal lattice. The compositions and lattice parameters of the studied samples are listed in Table 1.

NMR measurements on powder samples were performed in a Bruker SXP pulse spectrometer at frequencies $\omega/2\pi = 13.8$ MHz (^2D), 19.3 MHz (^{51}V) and 9–90 MHz (^1H). NMR spectra were recorded by integrating the echo signal and sweeping the magnetic field (^{51}V) and by Fourier transforming the free-induction decay signal (^1H). The ^1H and ^2D spin–lattice relaxation times T_1 were measured using the inversion–recovery method (pulse sequence 180°–τ–90°), while the ^{51}V T_1 was determined from the recovery of the echo signal after the saturation pulse sequence. The low temperature measurements were made in an Oxford Instruments CF1200 continuous flow helium cryostat. The sample temperature, monitored by a chromel/Au–Fe thermocouple, was stable to within 0.1 K. For $T > 290$ K we used a glass Dewar system with an air flow. In this range the temperature monitored by a copper/constantan thermocouple was stable to within 0.5 K.

3. Results

3.1. Phase boundaries

Information on the phase boundaries is important for the unambiguous interpretation of experimental data. The precipitation of the hydride phase can be detected by the appearance of a second relaxation time in the recovery of the longitudinal nuclear magnetization [5]. We have found hydride phase precipitation in b.c.c.-$TaV_2H_{2.3}$ below 170 K and in b.c.c.-$TaV_2D_{2.4}$ below 190 K. In the other samples no signs of phase transformation could be detected down to 100 K. These NMR observations have been confirmed by heat capacity measurements. Thus almost all the results to be discussed below correspond to the homogeneous solid solution (α) phase. The exception is the low temperature region for b.c.c.-$TaV_2H_x(D_x)$ with $x > 2$.

3.2. ^{51}V and ^1H Knight shifts

For all the studied samples the ^{51}V NMR spectrum at room temperature consists of a single line without any pronounced structure. The ^{51}V Knight shift values K_V have been determined from the positions of the line maxima with respect to the ^{51}V resonance line in an aqueous solution of $LiVO_3$. The measured ^{51}V Knight shift at room temperature as a function of the total H(D) content is shown in Fig. 1. It can be seen that K_V values at high x are considerably higher than those at low x. This trend is also characteristic for vanadium-based C15-type hydrides [9, 10]. For all x the ^{51}V Knight shift is nearly temperature independent.

The values of the proton Knight shift K_H have been determined from ^1H NMR spectra at room temperature, H_2O serving as the reference substance. We have corrected the data for demagnetization effects in powder samples using the expressions derived in ref. 11. The corrected values of K_H for different samples are shown in Fig. 2. It should be noted that the corrections are considerably lower than the range of $K_H(x)$ variations. For all the studied samples K_H is negative, the absolute value of the shift decreasing with increasing hydrogen concentration. This is in general agreement with the results obtained by Schmidt and Weiss [12] on b.c.c.-$Ta_{0.5}V_{0.5}H_x$ and b.c.c.-$Ta_{0.7}V_{0.3}H_x$. However, the behaviour of K_H for b.c.c.-TaV_2H_x differs qualitatively from that for C15-TaV_2H_x [4].

Figure 2 also shows the hydrogen concentration dependence of the ^1H NMR linewidth $\Delta\nu$ measured at $\omega/2\pi = 90$ MHz. For all the studied samples the di-

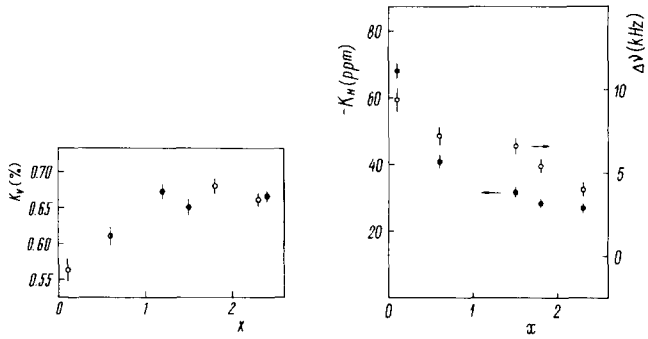

Fig. 1. ^{51}V Knight shift at room temperature as a function of the total H(D) content in b.c.c.-TaV_2. Open, filled and half-filled circles correspond to hydrided, deuterided and mixed isotope samples respectively.

Fig. 2. Proton Knight shift (●) and proton NMR linewidth (○) measured at $T = 295$ K and $\omega/2\pi = 90$ MHz as functions of the total H(D) content in b.c.c.-TaV_2.

pole–dipole interactions of ^{1}H spins at room temperature are averaged out owing to the fast hydrogen diffusion, and $\Delta\nu$ is determined by the distribution of demagnetization fields over the sample volume. Since the external magnetic field in the course of $\Delta\nu$ measurements was constant and the sample shapes were identical, the linewidth should be proportional to the magnetic susceptibility χ. Our results show that χ decreases with increasing hydrogen content. This is in a general agreement with the results of χ measurements in b.c.c.-TaV_2–H by the Faraday method [13]. However, our data indicate a more rapid decrease in χ as a function of x than those of ref. 13.

3.3. ^{51}V spin–lattice relaxation rate

The measured spin–lattice relaxation rate T_1^{-1} for host metal nuclei in metal–hydrogen systems usually results from the sum of contributions due to conduction electrons (T_{1e}^{-1}) and the effects of H(D) motion on magnetic dipole (T_{1d}^{-1}) and electric quadrupole (T_{1Q}^{-1}) interactions; hence

$$(T_1^{-1})_V = (T_{1e}^{-1})_V + (T_{1d}^{-1})_V + (T_{1Q}^{-1})_V \quad (1)$$

The conduction electron contribution can be obtained directly from the experimental $T_1^{-1}(T)$ data at low temperatures, where the motional contributions are negligible. In fact, for all the studied samples at $T<60$ K the ^{51}V relaxation rate is found to be proportional to the temperature. This linear temperature dependence is typical for the conduction electron (Korringa) contribution. The values of $(T_{1e}T)_V^{-1}$ obtained from the slopes of the $T_1^{-1}(T)$ dependences for different samples are presented in Fig. 3. It can be seen that $(T_{1e}T)_V^{-1}$ decreases with increasing H(D) content.

For the samples with high H(D) concentration the ^{51}V relaxation rate increases strongly at $T>100$ K and shows a maximum which is typical for the motional contributions. Examples of such behaviour are presented in Fig. 4. Estimates of the dipolar interaction between ^{51}V and ^{1}H (or ^{2}D) spins indicate that $(T_{1d}^{-1})_V$ is much smaller than the observed maximum values of the relaxation rate, *i.e.* the quadrupole interaction is primarily responsible for the observed $(T_1^{-1})_V$ maxima. Since the quadrupole relaxation mechanism is determined by charge fluctuations, the ^{51}V relaxation measurements can give direct information on isotope effects in H(D) motion [14]. The positions of the $(T_1^{-1})_V$ maxima in our deuterided samples are shifted to higher T with respect to those in the hydrided samples with nearly the same x. This is consistent with the normal isotope effect in hydrogen motion (the hopping rate for hydrogen is higher than for deuterium).

3.4. ^1H and ^2D spin–lattice relaxation rates

The measured proton spin–lattice relaxation rate in metal–hydrogen systems is usually taken to be the sum of the electronic (Korringa) term and the contribution due to dipole–dipole interaction modulated by hydrogen diffusion:

$$(T_1^{-1})_H = (T_{1e}^{-1})_H + (T_{1d}^{-1})_H \quad (2)$$

The electronic term proportional to T is expected to dominate at low temperatures. However, in contrast to the behaviour of ^{51}V relaxation rates, for all the studied samples we have found strong deviations from the Korringa temperature dependence of the ^{1}H relaxation rate in the low temperature region. Examples of the observed temperature dependence of $(T_1^{-1})_H$ at low T are shown in Fig. 5. Extrapolation of all the measured $T_1^{-1}(T)$ dependences to $T=0$ results in finite (and rather high) T_1^{-1} values. Moreover, for some of the samples a frequency dependence of $(T_1^{-1})_H$ has been found in the low temperature region. These features in the proton relaxation rate may result from the

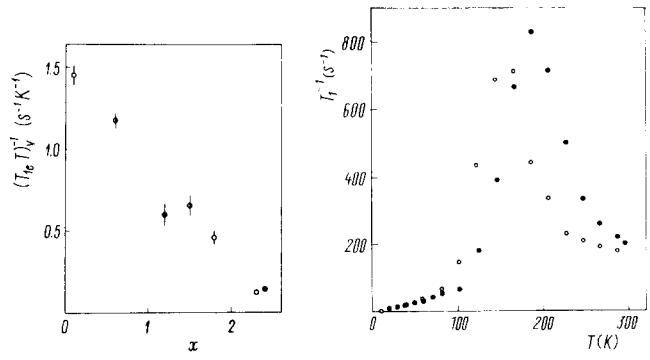

Fig. 3. Electronic contribution to ^{51}V spin–lattice relaxation rate as a function of the total H(D) content in b.c.c.-TaV_2. Open, filled and half-filled circles correspond to the hydrided, deuterided and mixed isotope samples respectively.

Fig. 4. Temperature dependence of ^{51}V spin–lattice relaxation rate in b.c.c.-$TaV_2D_{1.2}$ (●) and b.c.c.-$TaV_2H_{1.8}$ (○) measured at 19.3 MHz.

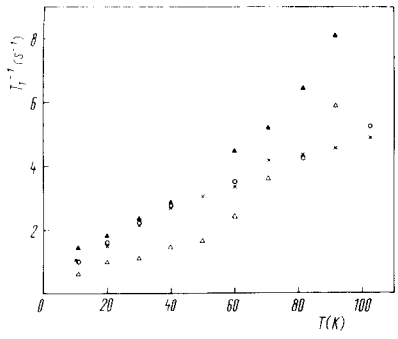

Fig. 5. Low temperature part of the temperature dependence of ^{1}H spin–lattice relaxation rates: ▲, b.c.c.-$TaV_2H_{0.1}$, $\omega/2\pi=45$ MHz; △, b.c.c.-$TaV_2H_{0.1}$, 90 MHz; ○, b.c.c.-$TaV_2H_{1.8}$, 90 MHz; ×, b.c.c.-$TaV_2H_{0.5}D_{1.0}$, 90 MHz.

effects of paramagnetic impurities [15] and/or from the mechanism of cross-relaxation between proton and quadrupolar nuclear spins [16]. In our case paramagnetic impurities are not the main source of the deviations from the Korringa behaviour. This is supported by the fact that for the C15-$TaV_2H_x(D_x)$ system prepared from the same starting materials we have not found any effects of impurities [2, 3]. Furthermore, the observed frequency dependence of $(T_1^{-1})_H$ at low T differs from that expected for the interaction between proton spins and paramagnetic impurities [15]. Following the arguments of ref. 16, we may conclude that the mechanism of cross-relaxation between proton and quadrupolar nuclear spins is primarily responsible for the observed deviations from the Korringa behaviour of $(T_1^{-1})_H$, since the b.c.c.-TaV_2–H(D) system (i) is a disordered one and (ii) contains ^{181}Ta nuclei with a large quadrupole moment. The cross-relaxation mechanism may result in the unusual (even non-monotonic) frequency dependence of $(T_1^{-1})_H$ at low T; at higher temperatures, at which hydrogen diffusion occurs on the NMR frequency scale, this contribution is removed [16]. Because of the cross-relaxation contribution, it is difficult to estimate the electronic term $(T_{1e}^{-1})_H$ from our low temperature proton relaxation data.

Figures 6–8 show the measured ^{1}H and ^{2}D spin–lattice relaxation rates for a number of b.c.c.-$TaV_2H_x(D_x)$ samples in the high temperature region. For each of the studied samples the relaxation rate exhibits a maximum which is typical for motional contributions to T_1^{-1}. For b.c.c.-$TaV_2H_x(D_x)$ this maximum can be attributed to the long-range hydrogen diffusion. In contrast to the case of C15-$TaV_2H_x(D_x)$ [2, 3], we have not found any signs of the additional low temperature T_1^{-1} maximum for b.c.c.-$TaV_2H_x(D_x)$. Thus we may conclude that the low temperature localized motion of H(D) (which is responsible for the additional T_1^{-1} maximum in C15-$TaV_2H_x(D_x)$ [3]) is lattice specific.

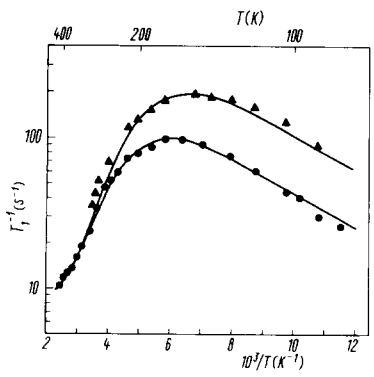

Fig. 6. Proton spin–lattice relaxation rates in b.c.c.-$TaV_2H_{0.1}$ measured at 9 MHz (▲) and 19.3 MHz (●) as functions of reciprocal temperature. Solid curves represent fits of the activation energy distribution model to the data (see Section 4.2).

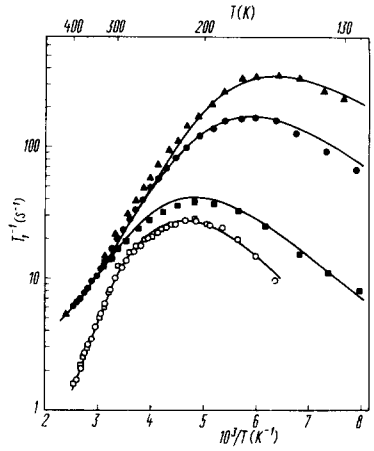

Fig. 7. ^{1}H and ^{2}D spin–lattice relaxation rates in b.c.c.-$TaV_2H_{1.8}$ (filled symbols), b.c.c.-$TaV_2D_{1.2}$ (○) and b.c.c.-$TaV_2D_{2.4}$ (□) as functions of reciprocal temperature. The relaxation rates are measured at 9 MHz (▲), 19.3 MHz (●) and 90 MHz (■) for ^{1}H and at 13.8 MHz for ^{2}D. Solid curves represent fits of the activation energy distribution model to the data (see Section 4.2).

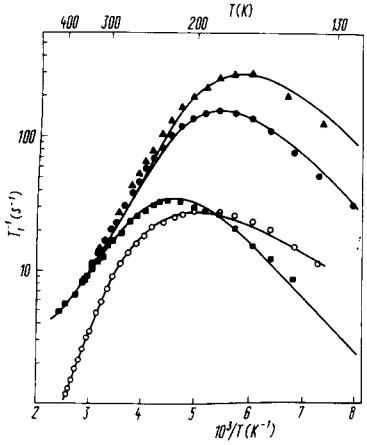

Fig. 8. ^{1}H and ^{2}D spin–lattice relaxation rates in b.c.c.-$TaV_2H_{0.5}D_{1.0}$ as functions of reciprocal temperature. Filled symbols correspond to ^{1}H relaxation rate measured at 9 MHz (▲), 17.9 MHz (●) and 90 MHz (■). Open circles correspond to ^{2}D relaxation rate measured at 13.8 MHz. Solid curves represent fits of the activation energy distribution model to the data (see Section 4.2).

The temperatures of the ^{1}H and ^{2}D relaxation rate maxima, T_{max}, and the maximum values of T_1^{-1} for all the studied samples are presented in Table 2. Also included in Table 2 are the values of T_{max} and $(T_1^{-1})^{max}$ for the C15-type systems $TaV_2H_{1.33}$ and $TaV_2D_{1.54}$ from ref. 3. We now summarize the main features of our high temperature relaxation data.

(1) The value of $(T_1^{-1})_H^{max}$ increases with increasing x, while $(T_1^{-1})_D^{max}$ is almost insensitive to changes in concentration.

(2) For each of the studied samples the low temperature slope of the log T_1^{-1} *vs.* T^{-1} plot is less steep

TABLE 2. Temperatures of the ^1H and ^2D spin–lattice relaxation rate maxima and maximum values of T_1^{-1}

Sample	Nucleus	$\omega/2\pi$ (MHz)	T_{max} (K)	$(T_1^{-1})^{max}$ (s^{-1})
b.c.c.-$TaV_2H_{0.1}$	^1H	19.3	160	98
b.c.c.-$TaV_2H_{0.2}D_{0.4}$	^1H	17.9	175	128
b.c.c.-$TaV_2H_{0.5}D_{1.0}$	^1H	17.9	185	155
b.c.c.-$TaV_2H_{1.8}$	^1H	19.3	169	163
b.c.c.-$TaV_2H_{2.3}$	^1H	19.3	181	190
C15-$TaV_2H_{1.33}$	^1H	19.3	290	110
b.c.c.-$TaV_2H_{0.2}D_{0.4}$	^2D	13.8	194	22.0
b.c.c.-$TaV_2D_{1.2}$	^2D	13.8	210	27.3
b.c.c.-$TaV_2H_{0.5}D_{1.0}$	^2D	13.8	204	27.4
b.c.c.-$TaV_2D_{2.4}$	^2D	13.8	207	28.0
C15-$TaV_2D_{1.54}$	^2D	13.8	300	9.7

than the high temperature one, and the frequency dependence of T_1^{-1} below T_{max} is much weaker than ω^{-2}. These features are often taken as evidence for the existence of a distribution of hydrogen hopping rates [17–19].

(3) The relaxation rate maximum for ^2D in b.c.c.-TaV_2D_x is shifted to higher temperatures than that for ^1H in b.c.c.-TaV_2H_x with nearly the same x. This is also true for the ^2D and ^1H relaxation rate maxima in the same sample with mixed isotope composition. The observed difference in the positions of $(T^{-1})_D$ and $(T_1^{-1})_H$ maxima is consistent with the normal isotope effect on the H(D) hopping rate.

(4) The high temperature slope of the log T_1^{-1} *vs.* T^{-1} plot for ^2D in b.c.c.-TaV_2D_x is higher than for ^1H in b.c.c.-TaV_2H_x with nearly the same x. This is also true for the ^2D and ^1H relaxation rates in the same sample with mixed isotope composition.

4. Discussion

4.1. Electronic properties

The magnetic susceptibility of a transition metal compound usually consists of three main contributions:

$$\chi = \chi_s + \chi_{orb} + \chi_d \tag{3}$$

where χ_s and χ_d are the spin susceptibilities of s- and d-electrons respectively and χ_{orb} is the orbital susceptibility of d-electrons. In a first approximation the spin contributions are proportional to the corresponding densities of electron states at the Fermi level, $N_s(E_F)$ and $N_d(E_F)$. The value of $N_d(E_F)$ is usually much higher than $N_s(E_F)$, *i.e.* $\chi_d \gg \chi_s$. For metal nuclei both K and $(T_{1e}T)^{-1}$ are determined by sums of the same contributions as χ and in the tight-binding approximation may be written as [20]

$$K_V = K_s + K_{orb} + K_d = \frac{1}{\mu_B N_A}(H_s\chi_s + H_{orb}\chi_{orb} + H_d\chi_d) \tag{4}$$

$$(T_{1e}T)_V^{-1} = (T_{1e}T)_s^{-1} + (T_{1e}T)_{orb}^{-1} + (T_{1e}T)_d^{-1}$$
$$= 2\hbar\gamma^2 k_B[H_s^2 N_s^2(E_F) + (pH_{orb}^2 + qH_d^2)N_d^2(E_F)] \tag{5}$$

where μ_B is the Bohr magneton, N_A is Avogadro's number, γ is the nuclear gyromagnetic ratio and H_s, H_{orb} and H_d are the appropriate hyperfine fields at nuclear sites (H_s and H_{orb} are positive, while the core polarization hyperfine field H_d is negative). The dimensionless factors p and q (not exceeding unity) are determined by admixture coefficients of different d-orbital states at the Fermi level.

When the values of χ, K_V and $(T_{1e}T)_V^{-1}$ show considerable temperature dependences, the orbital and spin contributions in eqns. (3)–(5) can be separated [21, 22]. Since in our system these values are found to be nearly temperature independent, we restrict ourselves to a qualitative analysis of the behaviour of $N(E_F)$ as a function of x. It can be seen that the expressions for χ and K_V contain both $N(E_F)$-dependent and $N(E_F)$-independent terms, while the expression for $(T_{1e}T)_V^{-1}$ contains only terms proportional to squares of the partial densities of states at the Fermi level. As the hydrogen content increases, the experimental values of χ and $(T_{1e}T)_V^{-1}$ decrease and those of K_V increase (Figs. 1–3). Taking into account that H_d in eqn. (4) is negative and assuming that the hyperfine fields at vanadium sites do not show strong changes in the studied range of x, we conclude that all the experimental data presented in Figs. 1–3 are consistent with the decrease in $N_d(E_F)$ with increasing x. This trend is common for hydrogen-containing group V metals [12]. Band structure calculations for these systems [12] also result in a decrease in $N(E_F)$ with increasing hydrogen content.

Although a detailed theory of hyperfine interactions of hydrogen dissolved in a metal is lacking, the experimental data on proton Knight shifts in transition metal hydrides [23–26] show unambiguously that K_H is determined mainly by the density of d-electron states at the Fermi level. Therefore K_H may be written in a form analogous to eqn. (4):

$$K_H = K_0 + \frac{1}{\mu_B N_A}\tilde{H}_d\chi_d \tag{6}$$

where $\tilde{H}_d$ is the effective hyperfine field at a proton site due to d-electrons. The value of $\tilde{H}_d$ may be roughly estimated from $\partial K_H/\partial\chi$ at low x (with hydrogen content as implicit parameter). Using the experimental values

of K_H (Fig. 2) and χ [13], we obtain $\tilde{H}_d \approx \mu_B N_A(\partial K_H/\partial\chi) = -4.2\times10^3$ Oe. Thus $\tilde{H}_d$ in b.c.c.-TaV_2H_x is negative, as in many other transition metal hydrides [24–26]. For C15-TaV_2H_x K_H is positive in the whole studied range of x and at low x both K_H and χ decrease with increasing hydrogen content [4]. The estimate of $\tilde{H}_d$ in C15-TaV_2H_x using the experimental data on K_H and χ [4] gives $\tilde{H}_d \approx 4\times10^2$ Oe, *i.e.* $\tilde{H}_d$ is positive. The difference in the signs of $\tilde{H}_d$ indicates that the spin (and probably the charge) distribution near protons in b.c.c.-TaV_2H_x differs significantly from that in C15-TaV_2H_x. This difference may be responsible for differences in the other properties of hydrogen in b.c.c.- and C15-TaV_2H_x.

4.2. *Diffusive motion of H(D) atoms*

The motional contribution to the proton spin–lattice relaxation rate, $(T_{1d}^{-1})_H$, originates from dipole–dipole interactions between different ^1H spins (HH) and between ^1H spins and host metal nuclear spins (HM). Using the standard equations [27], $(T_{1d}^{-1})_H$ can be expressed in terms of the spectral density functions for fluctuating dipolar fields. For the simplest model [28], known as the Bloembergen–Purcell–Pound (BPP) approximation, the spectral density functions are lorentzian and the motional contribution to the proton relaxation rate is given by

$$(T_{1d}^{-1})_H = (T_{1d}^{-1})_{HH} + (T_{1d}^{-1})_{HM} = \frac{4M_{2H}}{3\omega}\left(\frac{y}{4+y^2} + \frac{y}{1+y^2}\right) + \frac{M_{2M}}{2\omega}\left(\frac{y}{1+(1-\alpha)^2y^2} + \frac{3y}{1+y^2} + \frac{6y}{1+(1+\alpha)^2y^2}\right) \quad (7)$$

Here $y = \omega\tau_d$, τ_d being the mean dwell time of a hydrogen atom in an interstitial site; M_{2H} and M_{2M} are the contributions to the "rigid lattice" second moment of the ^1H NMR line from HH and HM dipolar interactions respectively,

$$M_{2H} = \tfrac{3}{5}\gamma_H^4\hbar^2 I_H(I_H+1)\sum_i r_i^{-6} \quad (8)$$

$$M_{2M} = \tfrac{4}{15}\gamma_H^2\gamma_M^2\hbar^2 I_M(I_M+1)\sum_j r_j^{-6} \quad (9)$$

where I_H and I_M are the spins and γ_H and γ_M are the gyromagnetic ratios for hydrogen and metal nuclei respectively; and $\alpha = \gamma_M/\gamma_H$. The summations $\sum_i r_i^{-6}$ and $\sum_j r_j^{-6}$ refer to sums over hydrogen and metal sites respectively, with the origin at a hydrogen site. All expressions apply to powder samples. In our case the role of metal nuclei is played by ^{51}V with $I_V = \frac{7}{2}$ and nearly 100% natural abundance.

According to eqn. (7), $(T_{1d}^{-1})_H$ is expected to have a maximum when $y \approx 1$. The precise value of y at which the $(T_{1d}^{-1})_H$ maximum is predicted depends on α and M_{2H}/M_{2M}. The asymptotic behaviour of $(T_{1d}^{-1})_H$ in the limits of fast ($y \ll 1$) and slow ($y \gg 1$) diffusion is given by

$$(T_{1d}^{-1})_H \propto \tau_d, \qquad y \ll 1 \quad (10)$$

$$(T_{1d}^{-1})_H \propto \omega^{-2}\tau_d^{-1}, \qquad y \gg 1 \quad (11)$$

If τ_d follows the Arrhenius relation

$$\tau_d = \tau_{d0}\exp(E_a/k_BT) \quad (12)$$

where E_a is the activation energy, then a plot of $\log(T_{1d}^{-1})_H$ *vs.* T^{-1} is expected to be linear in the fast diffusion and slow diffusion limits with the slopes E_a/k_B and $-E_a/k_B$ respectively. It should be noted that more accurate lattice-specific calculations of the spectral density functions (see *e.g.* ref. 29) lead to results that are close to the BPP predictions. In particular, the asymptotic behaviour of $(T_{1d}^{-1})_H$ in the framework of lattice-specific calculations can also be written in the form of eqns. (10) and (11).

However, our experimental $(T_1^{-1})_H$ results show strong deviations from the BPP predictions. As mentioned above, the asymmetric shape of the $\log(T_{1d}^{-1})_H$ *vs.* T^{-1} plot and the weak frequency dependence of $(T_{1d}^{-1})_H$ below T_{max} may indicate the existence of a distribution of τ_d values. Taking into account eqn. (12), the distribution of τ_d can be expressed as a distribution of E_a. In our case the existence of such a distribution seems to be quite natural, since in a disordered alloy hydrogen occupies a number of inequivalent interstitial sites formed by different combinations of metal atoms. The motional relaxation rate is then given by

$$T_{1d}^{-1} = \int T_{1d}^{-1}(E_a)G(E_a)\,dE_a \quad (13)$$

where $G(E_a)$ is the normalized distribution function of E_a values and $T_{1d}^{-1}(E_a)$ is defined by eqns. (7)–(9) and (12).

We have described our high temperature proton relaxation data in terms of the model using a gaussian distribution function $G(E_a)$. The model calculations are based on eqns. (2), (7), (12) and (13). The value of M_{2H} is calculated from eqn. (8) assuming random occupation of tetrahedral sites restricted by blocking effects [30], while M_{2M}, τ_{d0}, the average activation energy $\bar{E}_a$, the distribution width ΔE_a and the Korringa product $T_{1e}T$ are varied until the best fit to all the relaxation data at different frequencies is obtained. The results of this fitting procedure are shown as solid curves in Figs. 6–8; the fitting parameters $\bar{E}_a$, ΔE_a, τ_{d0} and $(T_{1e}T)^{-1}$ for all the samples are presented in Table 3. It should be stressed that the fits to the T_1^{-1} data

TABLE 3. Parameters resulting from the fit of the model using a gaussian distribution of activation energies to the ^{1}H and ^{2}D spin–lattice relaxation data

Sample	Nucleus	$\bar{E}_a$ (eV)	ΔE_a (eV)	τ_{d0} (s)	$(T_{1e}T)^{-1}$ (s^{-1} K^{-1})
b.c.c.-$TaV_2H_{0.1}$	^{1}H	0.11	0.036	2×10^{-12}	1.5×10^{-2}
b.c.c.-$TaV_2H_{0.2}D_{0.4}$	^{1}H	0.14	0.032	6×10^{-13}	1.4×10^{-2}
b.c.c.-$TaV_2H_{0.5}D_{1.0}$	^{1}H	0.15	0.022	7×10^{-13}	0.5×10^{-2}
b.c.c.-$TaV_2H_{1.8}$	^{1}H	0.13	0.022	1×10^{-12}	0.4×10^{-2}
b.c.c.-$TaV_2H_{2.3}$	^{1}H	0.12	0.026	2×10^{-12}	0.3×10^{-2}
C15-$TaV_2H_{1.33}$	^{1}H	0.21		2×10^{-12}	0.4×10^{-2}
b.c.c.-$TaV_2H_{0.2}D_{0.4}$	^{2}D	0.19	0.059	2×10^{-13}	
b.c.c.-$TaV_2D_{1.2}$	^{2}D	0.19	0.036	6×10^{-13}	
b.c.c.-$TaV_2H_{0.5}D_{1.0}$	^{2}D	0.19	0.046	4×10^{-13}	
b.c.c.-$TaV_2D_{2.4}$	^{2}D	0.19	0.036	6×10^{-13}	
C15-$TaV_2D_{1.54}$	^{2}D	0.23			

at different frequencies are made with the *same* set of parameters. As can be seen from Figs. 6–8, the model gives a satisfactory description of the experimental data in a wide frequency range.

An important contribution to the ^{2}D spin–lattice relaxation rate may arise from the interaction of nuclear quadrupole moments with electric field gradients (EFGs) modulated by deuterium diffusion. Since the gyromagnetic ratio of ^{2}D is considerably smaller than that of ^{1}H, the electronic and dipolar relaxation rates are less effective for ^{2}D and the ^{2}D relaxation in disordered metal–hydrogen systems is usually dominated by the quadrupolar contribution $(T_{1Q}^{-1})_D$. In random b.c.c. alloys the local symmetry of interstitial sites is non-cubic and the EFG on ^{2}D is produced mainly by the neighbouring metal atoms. This is supported by the fact that in our systems the maximum value of $(T_1^{-1})_D$ is almost insensitive to changes in deuterium concentration (see Table 2). The corresponding quadrupolar contribution to the relaxation rate is expected to have approximately the same temperature dependence as the dipolar deuterium–metal contribution [31, 32]. Hence the temperature dependence of $(T_1^{-1})_D$ in the limits of fast and slow diffusion allows one to determine the activation energy for deuterium diffusion. However, as has been noted by Seymour [31], it is difficult to obtain a reliable estimate of τ_d at the temperature of the $(T_{1Q}^{-1})_D$ maximum. The theoretical estimation of the maximum T_{1Q}^{-1} value is also problematic since it requires knowledge of the spatial charge distribution and the antishielding factor for a given metal–hydrogen system. It should be noted that in our mixed isotope systems the hopping of neighbouring H atoms has a negligible effect on ^{2}D relaxation, since the EFG on ^{2}D is produced mainly by metal atoms. This means that the values of E_a and τ_{d0} obtained from the analysis of the ^{2}D relaxation data characterize the motion of D atoms, not the neighbouring H atoms. Similar arguments are also applicable to the case of ^{1}H relaxation in the mixed isotope samples, since in our systems $(T_{1d}^{-1})_H$ appears to be dominated by the $(T_{1d}^{-1})_{HM}$ contribution.

For the analysis of the ^{2}D relaxation data we have used the same approach as for the proton relaxation, assuming that $(T_{1Q}^{-1})_D$ is proportional to the dipolar relaxation rate. As noted above, this can hardly result in reliable values of τ_{d0}; however, the values of $\bar{E}_a$ and ΔE_a are expected to be accurate. The results of the fitting are shown as solid lines in Figs. 7 and 8; the fitting parameters for deuterium are presented in Table 3. The Korringa contributions for ^{2}D are found to be negligible in the studied temperature range. Also included in Table 3 are the fitting parameters for H(D) diffusion in the C15-type systems $TaV_2H_{1.33}$ and $TaV_2D_{1.54}$ from ref. 3.

As can be seen from Table 3, the electronic contribution $(T_{1e}T)_H^{-1}$ decreases with increasing total H(D) concentration. This is consistent with the behaviour of $(T_{1e}T)_V^{-1}$. Moreover, $(T_{1e}T)_H^{-1}$ appears to be nearly proportional to $(T_{1e}T)_V^{-1}$, so that $(T_{1e}T)_H^{-1}/(T_{1e}T)_V^{-1} \approx 0.01$ for all the studied samples with $x<2$. The value of $\bar{E}_a$ for b.c.c.-$TaV_2H_{0.1}$ lies between the values of E_a for TaH_x and VH_x as $x\to0$ (0.14 and 0.06 eV respectively [33]). The concentration dependence of $\bar{E}_a$ for hydrogen in b.c.c.-TaV_2H_x follows the general trends observed for the α phase of b.c.c. metal–hydrogen systems [33]: with increasing x the activation energy first increases, then levels off and tends to decrease at H:M > 0.6. The values of the distribution width ΔE_a for our system are of the same order of magnitude as those obtained for b.c.c.-$V_zNb_{1-z}H_{0.2}$ [5]. However, the average hopping rates (and therefore the hydrogen mobilities) in b.c.c.-TaV_2–H are considerably higher than in b.c.c.-V_zNb_{1-z}–H with comparable hydrogen concentration. This is indicated by the lower T_{max} values for the b.c.c.-TaV_2–H system. Comparison of the hy-

drogen diffusion parameters in $TaV_2H_x(D_x)$ with C15 and b.c.c. structures shows that for the b.c.c. system the activation energy is much lower and the long-range diffusion is much faster than for the C15 counterpart (Tables 2 and 3).

For all the studied samples there is a marked isotope effect on the activation energy: $\tilde{E}_a^D > \tilde{E}_a^H$ (see Table 3). This sign of the isotope effect on E_a is typical for hydrogen in b.c.c. metals [34]. It should be noted that the inequality $\tilde{E}_a^D > \tilde{E}_a^H$ is retained for the diffusion of hydrogen and deuterium in the same mixed isotope sample, the values of $\tilde{E}_a^{H(D)}$ being close to the corresponding values for a fully hydrided (deuterided) system. Fukai and coworkers [35, 36] have found from their NMR measurements on NbH_xD_z and TaH_xD_z that the diffusion of both hydrogen and deuterium in the same mixed isotope sample is characterized by the same E_a value, although in the binary systems NbH_{x+z} (NbD_{x+z}) and TaH_{x+z} (TaD_{x+z}) there is a considerable difference between E_a^H and E_a^D. These results have led the authors [35, 36] to the conclusion that the motion of H atoms in niobium and tantalum should be strongly correlated. Our measurements do not support the picture of strongly correlated hydrogen diffusion in b.c.c. metals. In fact, our results indicate that even at high hydrogen concentration (H:M ≈ 0.5) the diffusion can be described as a single-particle process.

5. Conclusions

The main results of our NMR measurements in the random b.c.c.-TaV_2–H(D) system may be summarized as follows.

The density of d-electron states at the Fermi level decreases with increasing H(D) content. In contrast to C15-TaV_2H_x, the effective hyperfine magnetic field at proton sites in b.c.c.-TaV_2H_x is negative (*i.e.* antiparallel to the external field).

The ^1H and ^2D spin–lattice relaxation data can be satisfactorily described in terms of the BPP model using a gaussian distribution of activation energies. The average value of the activation energy for hydrogen diffusion initially increases with increasing x, but at $x \gtrsim 1.5$ starts to decrease. The long-range diffusion of H(D) in b.c.c.-$TaV_2H_x(D_x)$ is much faster than in C15-$TaV_2H_x(D_x)$. In contrast to the case of C15-$TaV_2H_x(D_x)$ [2, 3], we have not found any signs of low temperature localized hydrogen motion in b.c.c.-$TaV_2H_x(D_x)$.

The average activation energy shows a distinct isotope effect: $\tilde{E}_a^D > \tilde{E}_a^H$. The same inequality is valid for diffusion of hydrogen and deuterium in a single sample with mixed isotope composition. This is consistent with the absence of strong correlation effects in the motion of H(D).

Acknowledgment

We are grateful to N. I. Kourov for the heat capacity measurements on our samples.

References

1 J. F. Lynch, *J. Phys. Chem. Solids, 42* (1981) 411.
2 A. V. Skripov, M. Yu. Belyaev, S. V. Rychkova and A. P. Stepanov, *J. Phys.: Condens. Mater, 1* (1989) 2121.
3 A. V. Skripov, S. V. Rychkova, M. Yu. Belyaev and A. P. Stepanov, *J. Phys.: Condens. Mater, 2* (1990) 7195.
4 A. V. Skripov, M. Yu. Belyaev, K. N. Mikhalev and A. P. Stepanov, *J. Alloys Comp., 177* (1991) 63.
5 L. Lichty, J. Shinar, R. G. Barnes, D. R. Torgeson and D. T. Peterson, *Phys. Rev. Lett., 55* (1985) 2895.
6 G. G. Libowitz and A. J. Maeland, *Mater. Sci. Forum, 31* (1988) 177.
7 Y. Fukai and H. Sugimoto, *Adv. Phys., 34* (1985) 263.
8 R. Messer, A. Blessing, S. Dais, D. Höpfel, G. Majer, C. Schmidt, A. Seeger, W. Zag and R. Lässer, *Z. Phys. Chem. N.F., Suppl. H.2,* (1986) 61.
9 M. Yu. Belyaev, A. V. Skripov, A. P. Stepanov and E. V. Galoshina, *Fiz. Met. Metalloved., 63* (1987) 905 (Engl. transl. *Phys. Met. Metallogr., 63*(5) (1987) 64).
10 A. P. Stepanov, A. V. Skripov and M. Yu. Belyaev, *Z. Phys. Chem. N.F., 163* (1989) 603.
11 R. Göring and B. Schnabel, *Ann. Phys. (Lpz.), 39* (1982) 301.
12 P. C. Schmidt and A. Weiss, *Z. Phys. Chem. N.F., 163* (1989) 597.
13 J. F. Lynch, R. Lindsay and R. O. Moyer, *Solid State Commun., 41* (1982) 9.
14 M. Yu. Belyaev, A. V. Skripov, V. N. Kozhanov and A. P. Stepanov, *Fiz. Tverd. Tela, 26* (1984) 2120 (Engl. transl. *Sov. Phys. – Solid State, 26* (1984) 1285).
15 T. T. Phua, B. J. Beaudry, D. T. Peterson, D. R. Torgeson, R. G. Barnes, M. Belhoul, G. A. Styles and E. F. W. Seymour, *Phys. Rev. B, 28* (1983) 6227.
16 L. R. Lichty, J. W. Han, D. R. Torgeson, R. G. Barnes and E. F. W. Seymour, *Phys. Rev. B, 42* (1990) 7734.
17 J. Shinar, D. Davidov and D. Shaltiel, *Phys. Rev. B, 30* (1984) 6331.
18 J. T. Markert, E. J. Cotts and R. M. Cotts, *Phys. Rev. B, 37* (1988) 6446.
19 A. V. Skripov, S. V. Rychkova, M. Yu. Belyaev and A. P. Stepanov, *Solid State Commun., 71* (1989) 1119.
20 A. Narath, in A. J. Freeman and R. B. Frankel (eds.), *Hyperfine Interactions,* Academic, New York, 1967, p. 287.
21 G. C. Carter, L. H. Bennett and D. J. Kahan, *Metallic Shifts in NMR, Part 1,* Pergamon, Oxford, 1977.
22 A. V. Skripov and A. P. Stepanov, *Phys. Status Solidi B, 126* (1984) 557.
23 R. M. Cotts, in G. Alefeld and J. Völkl (eds.), *Hydrogen in Metals 1,* Springer, Berlin, 1978, p. 227.
24 S. Kazama and Y. Fukai, *J. Phys. Soc. Jpn., 42* (1977) 119.
25 R. Göring, R. Lukas and K. Bohmhammel, *J. Phys. C: Solid State Phys., 14* (1981) 5675.
26 R. C. Bowman, E. L. Venturini, B. D. Craft, A. Attalla and D. B. Sullenger, *Phys. Rev. B, 27* (1983) 1474.
27 A. Abragam, *The principles of Nuclear Magnetism,* Clarendon, Oxford, 1961.
28 N. Bloembergen, E. M. Purcell and R. M. Pound, *Phys. Rev., 73* (1948) 679.

29 D. A. Faux, D. K. Ross and C. A. Sholl, *J. Phys. C: Solid State Phys., 19* (1986) 4115.
30 A. C. Switendick, *Z. Phys. Chem. N.F., 117* (1979) 89.
31 E. F. W. Seymour, *J. Less-Common Met., 88* (1982) 323.
32 N. Salibi, B. Ting, D. Cornell and R. E. Norberg, *Phys. Rev. B, 38* (1988) 4416.
33 E. H. Sevilla and R. M. Cotts, *J. Less-Common Met., 129* (1987) 223.
34 J. Völkl and G. Alefeld, in G. Alefeld and J. Völkl (eds.), *Hydrogen in Metals 1,* Springer, Berlin, 1978, p. 321.
35 Y. Fukai, K. Kubo and S. Kazama, *Z. Phys. Chem. N.F., 115* (1979) 181.
36 S. Kazama and Y. Fukai, *Proc. Int. Symp. JIMIS-2: Hydrogen in Metals, Sendai, Suppl. Trans. JIM, 21* (1980) 173.